Development and assessment of a hybrid breakwater-integrated wave energy converter

Tomás Calheiros-Cabral, Ajab G. Majidi, Victor Ramos, Gianmaria Giannini, Paulo Rosa-Santos, and Francisco Taveira-Pinto

Abstract— **Harnessing and using marine renewable energy at seaports is a promising solution to put these energy-intensive infrastructures on the right track to energy self-sufficiency and environmental sustainability, reducing their carbon footprint. This paper presents a summary of the main conclusions and achievements of a recently concluded R&D project that encompassed the experimental study of an innovative hybrid wave energy converter integrated into a case-study rubble-mound breakwater in the Port of Leixões, Portugal. It also describes the prospective studies planned in two ongoing projects, PORTOS – Ports Towards Energy Self-Sufficiency and WEC4Ports – A hybrid Wave Energy Converter for Ports, intended to further develop and assess this promising technology. It has been demonstrated that its wave-to-wire efficiency and annual energy production are 27.3% and 35.0 MWh/m per year, respectively, for the case-study location. Hence, a 240 m long device could provide more than half of the port's electricity consumption, which vows for the device's potential. Moreover, the impact of its integration into the case-study breakwater showed that it leads to a 50% reduction of overtopping discharges over the structure, and no significant effects on the structure's wave reflection, although the stability of the toe berm blocks was negatively impacted. Overall, the conclusions obtained are favourable to the integration of this technology into rubble-mound breakwaters. Notwithstanding, further research is still needed, namely in terms of wave forces acting upon the structure, important for the assessment of the functional performance and lifecycle readiness of the technology, and the use of PTO control strategies. This is being addressed in PORTOS and WEC4Ports projects.**

Keywords—**Blue Ports, Oscillating Water Column, breakwater stability, Overtopping WEC, Energy self-sufficiency.**

I. Introduction

DUE to the stochastic nature of renewable resources, they aren't always capable of offering electricity and covering demand while needed. Higher scenarios of renewable integration have been proposed, and the principal challenge for better penetration is generally their perceived consequences on the stableness of the electric grid. To help withinside the version of renewables options that lessen traditional fuel intake and increase electricity independence, answers which include storage and/or mainland interconnection have been suggested. There are significant economic elements to be taken into consideration with the destiny boom of renewable energy expected. They are related to the infrastructure that has to keep an uninterrupted energy delivery and the price of electricity. The often-overlooked wave energy is a renewable high-density resource that can contribute to the ambitious Europe decarbonization targets to become the world's first climate-neutral continent, as predicted in the EU Green Deal [1].

The technical solutions of wave energy converters (WEC) are mature to some extent, but the present state of the art indicates that these technologies are still far from the stage of real engineering applications (reasonable payback) [2-4]. The high construction, maintenance and installation costs of WECs originated from the harsh marine conditions may directly lead to an uneconomic price of electric power. Therefore, the integration of some

Submitted 30 December, 2021; published 19 December 2022.

This research was supported by the OCEANERA-NET project SE@PORTS—Sustainable Energy at Sea PORTS (ref. OCEANERA/0004/2016), funded by FCT, the Portuguese Foundation for Science and Technology, by the project PORTOS—Ports Towards Energy Self-Sufficiency (ref. EAPA_784/2018) and co-financed by the Interreg Atlantic Area Program through the European Regional Development Fund, and also by the project WEC4Ports – A hybrid Wave Energy Converter for Ports (OCEANERA-NET COFUND) ref. OCEANERA/0004/2019, also funded under the frame of FCT.

T. Calheiros-Cabral, A. G. Majidi, V. Ramos, G. Giannini, P. Rosa-Santos and F. Taveira-Pinto, are with FEUP—Faculty of Engineering of the University of Porto, Department of Civil Engineering, Rua Dr. Roberto Frias, s/n, 4200-465 Porto, Portugal and CIIMAR, Interdisciplinary Centre of Marine and Environmental Research of the University of Porto, Terminal de Cruzeiros do Porto de Leixões, Avenida General Norton de Matos, s/n, 4450-208 Matosinhos, Portugal (e-mails: tcabral@fe.up.pt; ajabgulmajidi@gmail.com jvrc@fe.up.pt; gianmaria@fe.up.pt; pjrsantos@fe.up.pt; fpinto@fe.up.pt).

Digital Object Identifier: https://doi.org/10.36688/imej.5.281-291

of these technologies into coastal protection structures [5] and harbour breakwaters [6] can be vital points of interest, like sharing the structure costs, accessibility of grid connection, generating currents in the interior harbour field, easy maintenance, and improvement in the performance of the protection structures due to the efficient absorption of wave energy [6, 7]. Besides, a significant decrease in greenhouse gas emissions and air pollution will occur on account of the contribution of the energy output of a harbour breakwater-integrated hybrid WEC to the highly consumed and usually non-renewable energy of harbours.

The present paper focuses on the main conclusions of the development of a harbour rubble-mound breakwater integrated overtopping and oscillating water column hybrid technology (h-WEC) [8-11]. These studies have shown that the annual energy production of the h-WEC investigated at the Port of Leixões, considering the efficiency of hydro and air turbines, presents promising results.

II. Case-Study Harbour Breakwater, Design and Optimization of the h-WEC

A. Location and characteristics of the case-study breakwater

The Port of Leixões is located on the northwest coast of Portugal, in the city of Porto. To ensure that it can handle the ever-larger ships that drive the sea shipping economy, a 300 m extension of the main breakwater is being developed by the Port Authority of Leixões, which creates a perfect opportunity for the incorporation of a wave energy harnessing device, such as the h-WEC, into the port's infrastructure. Therefore, the h-WEC was designed to flawlessly integrate the planned extension of the North breakwater of the Port of Leixões, Fig. 1, although it can be easily adapted to fit multiple other rubble-mound breakwaters. The middle section of the extension was chosen for the integration of a 20 m-wide module that was posteriorly tested using physical modelling, at a water depth of 17.5 m. This section has a *tout-venant* core, two rockfill filter layers and a two blocks thick armour layer of regularly placed high-density Antifer blocks, Fig. 1b.

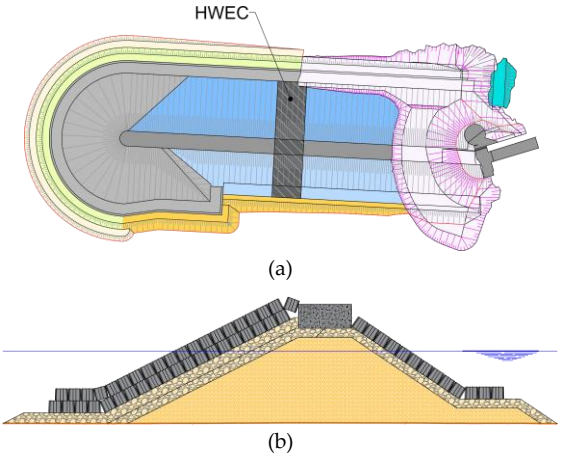

Fig. 1. Planned extension of the North breakwater of the Port of Leixões: (a) plan view and (b) cross section.

The Port of Leixões is exposed to an energetic wave climate [10], which warrants the high energy harvesting potential of the location but also renders the assessment of the stability and functionality of the breakwater a critical aspect of the h-WEC's design. Hence, the wave climate was characterized by propagating waves from offshore to the approximate location of the extension, at a water depth of around 21 m (CD), using the SWAN model [12, 13]. The total mean annual resource available is estimated at 16.9 kW/m. Following the recommendations by [14], seven representative sea states were chosen for physical model testing, Fig. 2. These were combined with three characteristic water levels determined from the Leixões tidal gauge over approximately five years, corresponding to the mean sea level (MSL) – 17.5 m (C.D.), a characteristic low water level (LWL) – 16.2 m (C.D.) and high water level (HWL) – 19.2 m (C.D.), with the associated probabilities of occurrence, 57.1%, 23.9% and 19.0%, respectively [10].

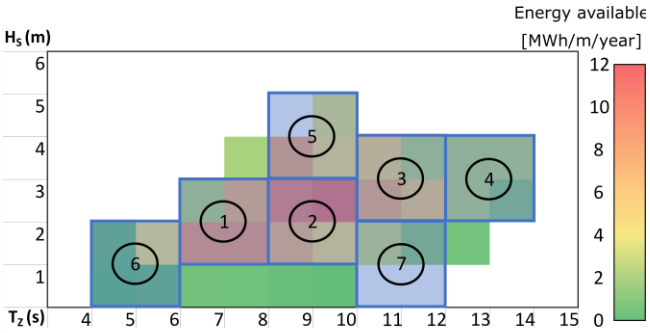

Fig. 2. Resource matrix at the site and seven selected sea states.

The selected sea states cover 97% of the annual available energy and 84% of the occurrences. Their characterising parameters are shown in Table I, in prototype values, where H_S represents the significant wave height and T_P the peak wave period.

TABLE I
CHARACTERIZING PARAMETERS OF THE SELECTED SEA STATES.

Sea state	H_S [m]	T_P [s]	Energy contribution [%]	Probability of occurrence [%]
SS1	1.7	9.0	19.6	25.6
SS2	1.9	11.5	24.5	20.5
SS3	2.8	14.1	19.0	6.2
SS4	2.9	16.6	10.5	2.6
SS5	3.7	11.6	13.8	3.1
SS6	1.1	6.8	4.9	21.0
SS7	1.5	13.9	4.6	5.1

B. Design of the h-WEC

One of the main obstacles hindering the successful implementation of wave energy into the main power grids of ocean-facing nations is the high cost of the produced electricity, as the Levelized Cost of Energy (LCoE) is still higher than most renewable and non-renewable alternatives. Notwithstanding, the LCoE of wave and tidal stream energy is expected to decrease 75% in the next ten years [15] making them commercially attractive and cost-competitive. Two critical factors to reduce the energy cost are to increase the efficiency and consistency of the devices' electricity production, as well as reducing

construction and maintenance costs. For that purpose, the hybridisation of two wave energy harvesting concepts was implemented in the design of the h-WEC in order to tackle the challenge of efficiency and consistency. Furthermore, the advantages of the integration of WECs into harbour breakwaters are explored, contributing to the reduction of construction and maintenance costs by sharing these with harbour structures, which implies the conceptualization of a device that can be seamlessly integrated into conventional rubble-mound breakwaters. Within this context, the selection of the technologies was performed by means of a decision matrix comparing four concepts, Fig. 3, taking into consideration cost-effectiveness, breakwater construction and integration, Technology Readiness Level (TRL), scalability and modularity, maintenance, reliability, and innovation. Hence, the h-WEC explores the added benefits of the hybridisation of two well-known and proven technologies to harvest the power of ocean waves, the Oscillating Water Column and the OverTopping Device, Fig. 3d.

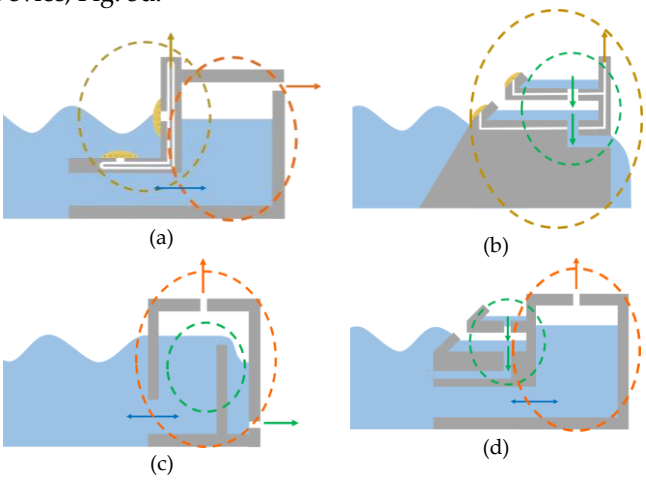

Fig. 3. Combination of (a) flexible membranes and OWC, (b) flexible membranes and OTD, (c) and (d) OWC and OTD.

1) OTD component design and optimization

The OTD component of the h-WEC was optimized by an evolutionary optimization algorithm that maximised the overall hydraulic efficiency by changing the crest height of the OTD's reservoirs according to set constraints, such as a minimum distance between reservoirs slabs of 1.25 m to facilitate access, a minimum height for the lowermost reservoir of 0.75 m to ensure a minimum hydraulic head for the turbines and uppermost reservoir's crest below the breakwater's crest level. Moreover, the overall hydraulic efficiency of a three-, four- and five-reservoirs device was compared. Extra reservoirs allow increasing the device's efficiency as they mitigate the negative effect of broad tidal ranges [6], despite adding construction and equipment's costs. The mean overtopping flow was calculated using the empirical expression developed by Kofoed [16], which is a function of the significant wave height tested and the reservoirs' crest levels.

The hydraulic efficiency is calculated as the ratio between the mean power captured by the OTD component and the mean power available in the considered sea state. The optimization covered the seven selected sea states and nine representative water levels, each with the associated number of hours of occurrence per year [17]. The obtained crest heights of the reservoirs were then studied using the software WOPSim 2.0 [18], and a hydraulic efficiency of 28.5% was calculated for a 4-reservoirs device (against 23.2% and 29.9% for a 3- and 5-reservoirs device, respectively). Hence, taking also into consideration the added costs of extra reservoirs, a 4-reservoirs device was chosen, with reservoirs' crests at 0.75, 2.00, 3.25 and 5.00 m (MSL) and ramp angles of 30°.

2) OWC component design optimization

The performance of OWC devices is very dependent on the wave frequency at which they are excited [19]. When a system is resonating with the incident waves, motions tend to be amplified, resulting in large accelerations and forces [14]. Different geometries of the OWC's chamber were designed to adjust the device's resonant frequency to match the most frequent peak wave periods at the location, leading to higher efficiencies, using Ansys Fluent [20]. However, as the modifications in the OTD's frontal ramp can lead to a decrease in its hydraulic efficiency, three different geometries, from A to C, were tested to determine the best overall efficiency of the h-WEC, Fig. 4.

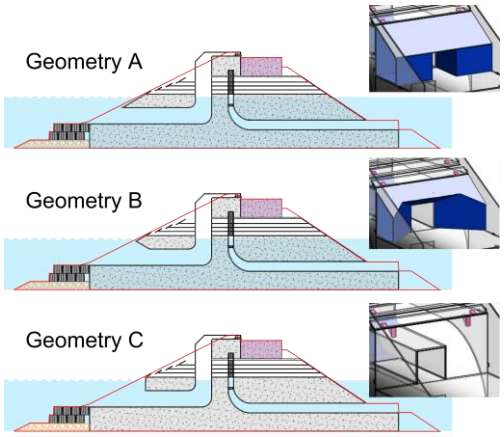

Fig. 4. Three geometries tested to determine the best overall efficiency, with the breakwater's cross-section contour in red.

III. PHYSICAL MODEL TESTS SETUP

A 40 cm wide physical model of the designed h-WEC was built in polymethyl methacrylate, at a geometric scale of 1:50, taking into consideration the facilities' limitations, similar studies [7, 21, 22] and other recommendations [23], Fig. 5a. The overtopping volumes into the OTD's reservoirs' were measured using the method described in [10]. The water that overtopped the device's crest was also captured and the total overtopped volume was measured using the same system.

Air compressibility is not adequately represented in physical models of OWC devices when the Froude similarity is used [24]. However, by connecting a rigid air reservoir of specified volume to the OWC chamber, air compressibility was correctly modelled following the methodology in [24]. Furthermore, the OWC's PTO was modelled using the diaphragm of a camera lens, which

works as an orifice plate, that has the same relation between flow rate and pressure as a biradial turbine [25], the one chosen for the PTO of the OWC component of the h-WEC. The diaphragm was controlled electronically during the tests, allowing to test different damping values (diaphragm apertures) expeditiously. The tested orifice diameters were 3.3, 6.3, 8.0, 11.4 and 14.0 mm.

The device was then tested in the wave basin of the Hydraulics, Water Resources and Environment Division of the Faculty of Engineering of the University of Porto, integrated into an 84 cm wide section of a model of the planned extension of the breakwater, Fig. 5b. The bathymetry was approximately reproduced by a 12.65 m long ramp with a 0.63° slope. Five wave gauges monitored the water's free surface elevation during the tests, and a sixth gauge measured the water's free surface oscillation inside the OWC chamber, Fig. 5c. In addition, a pressure sensor recorded the air pressure variation at the exit of the OWC, from which the airflow rate was determined [25].

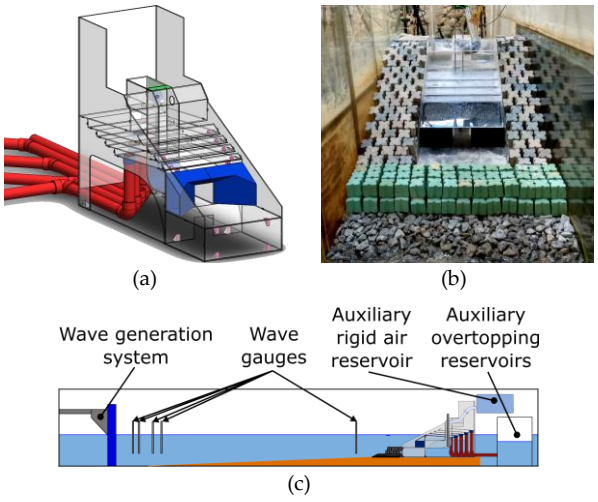

Fig. 5. (a) 3D model of the h-WEC (geometry B only), (b) physical model of the h-WEC integrated into a section of the breakwater, and (c) wave channel configuration.

The tests were carried out with regular and irregular waves. The height of the tested regular waves was 0.02 m and the wave period ranged from 0.8485 to 2.121 s with 0.141 s increments (*i.e.*, 6 to 15 s with 1 s increments in full-scale values). After these, tests were carried out with wave heights of 0.04 and 0.08 m, but the natural resonant period of the device, for each geometry, was determined in the tests with H=0.02 m. All the tests with regular waves were carried out with the MSL (0.488 m of water depth, 0.350 m at the toe of the breakwater) and lasted 400 waves each, Table II.

The tests with irregular waves were carried out using a JONSWAP spectrum with a peak enhancement factor of 3.3. The conditions considered are depicted in Table III. The tests were carried out with the LWL, the MSL and the HWL, and each test lasted 512 waves.

The significant wave heights and peak wave periods tested to assess the impact of the h-WEC in the breakwater's stability and functionality are detailed in Table IV. These tests were carried out for the LWL and HWL only, as these are the most critical, lasted 1024 waves, and were carried out with and without the h-WEC integrated into the breakwater. Conditions were limited by the depth induced wave breaking and the wave generation system's limitations. For clarity, the wave periods tested will be presented and discussed in prototype values.

TABLE II
TEST PROGRAM WITH REGULAR WAVES.

Condition	H [m]	T [s]
RW1	0.02	0.8485
RW2	0.02	0.9899
RW3	0.02	1.131
RW4	0.02	1.273
RW5	0.02	1.414
RW6	0.02	1.556
RW7	0.02	1.697
RW8	0.02	1.838
RW9	0.02	1.980
RW10	0.02	2.121
RW11	0.02	T_R [1] + 0.071
RW12	0.02	T_R - 0.071
RW13	0.04	T_R
RW14	0.08	T_R

[1] Resonant wave period.

TABLE III
TEST PROGRAM WITH IRREGULAR WAVES

Condition	H_S [m]	T_P [s]	Energy contribution [%]	Probability of occurrence [%]
IW1	0.034	1.273	19.6	25.6
IW2	0.038	1.626	24.5	20.5
IW3	0.056	1.994	19.0	6.2
IW4	0.058	2.348	10.5	2.6
IW5	0.074	1.640	13.8	3.1
IW6	0.022	0.962	4.9	21.0
IW7	0.030	1.966	4.6	5.1

TABLE IV
TEST PROGRAM FOR STABILITY AND FUNCTIONALITY ANALYSIS

Condition	H_S [m]	T_P [s]	Repetitions	Water level
SF1	0.120	1.838	1	
SF2	0.160	2.263	2	LWL
SF3	0.190	2.263	2	
SF1	0.120	1.838	1	
SF2	0.160	2.263	2	HWL
SF3	0.190	2.263	4	

IV. WAVE ENERGY HARVESTING EFFICIENCY AND ESTIMATED ANNUAL ELECTRICITY PRODUCTION

A. *Wave energy harvesting efficiency*

The hydrodynamic behaviour of the device was characterized by means of the tests with regular waves, as it allowed to highlight the effect of wave height and period on its performance. The resonant period of the OWC was determined for each tested geometry, and the overall hydrodynamic efficiency of the device was determined. The results will be presented for each component individually, and then for the h-WEC as a whole.

1) *Analysis of the OWC component*

The resonant frequency of the OWC was determined for the three tested geometries with a precision of 1 s (full-

scale). Afterwards, the precision was increased to 0.5 s by testing the device for the same wave height and two wave periods: the resonant period plus and minus 0.5 s. This was done for the three geometries, and the Response Amplitude Operator (RAO) was calculated, determined as the ratio between the amplitude of the water's free surface oscillation inside the OWC chamber and the incident wave height. Fig. 6a shows the results obtained.

The resonant period of geometry A, B and C for the MSL was 12.5, 11.5 and 10.5 s, respectively. As expected, the resonant wave period decreased from geometry A to B to C. The variation of the RAO with increasing wave height was then assessed by testing each geometry for wave heights of 0.04 m and 0.08 m for their respective resonant wave periods, Fig. 6b.

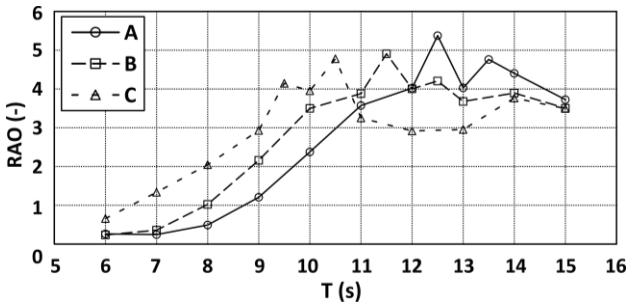

(a)

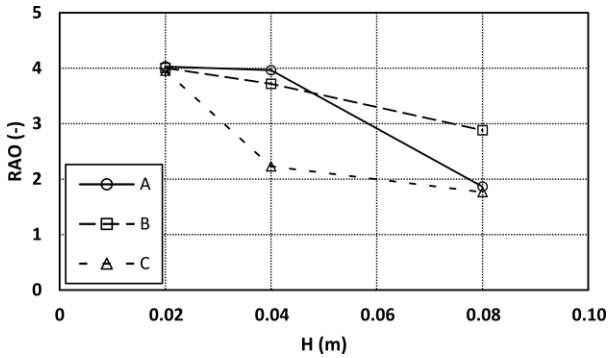

(b)

Fig. 6. Response Amplitude Operator for geometries A, B and C for (a) a fixed wave height of 0.02 m and (b) a fixed wave period, equal to each geometry's resonant period. Wave period values are in full-scale.

The RAO decreases with increasing wave height, similarly to what was observed by [26] and [27]. This is attributed to an increase in chamber free surface deformation and water sloshing as wave height increases [26], as well as a higher dissipation of the wave energy in the motion [9].

The hydrodynamic power captured by the OWC component was then computed as,

$$P_{OWC} = \frac{pA_c \frac{\partial \eta}{\partial t}}{W} \quad (1)$$

where p (Pa) is the instantaneous air pressure drop between the chamber of the OWC and the exterior, A_c (m²) the cross-section of the free surface inside the OWC chamber, in this case, 0.10 m × 0.10 m, η (m) the water's free surface oscillation inside the OWC chamber, t (s) the time and W (m) the width of the OWC chamber, in this case, 0.10 m (model values).

The capture width ratio (CWR), or hydrodynamic efficiency, is the ratio between the hydrodynamic power captured and the power available. A 0.10 m wavefront was considered to calculate the wave power available for the OWC, Fig. 7, as this allows a more adequate comparison with CWR values for other OWC devices obtained from the literature, instead of considering the full width of the h-WEC (0.40 m).

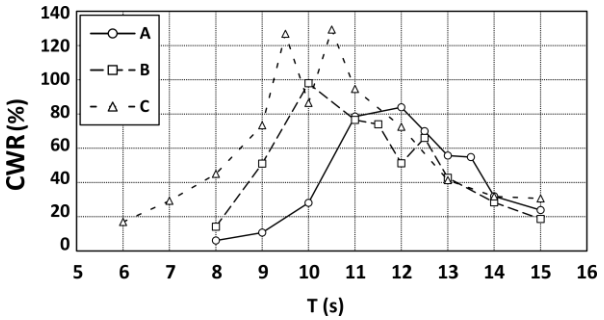

Fig. 7. Capture width ratio of the OWC as a function of wave period (full-scale values) for H=0.02 m.

The CWR of the OWC peaks close to its natural resonant period for the three geometries. The highest CWR is obtained for T=12.0 s for geometry A, T=10.0 s for geometry B and T=10.5 s for geometry C. However, the CWR of geometry C presents two peaks, one for T=9.5 s and one for T=10.5 s, with a decrease in efficiency for T=10.0 s. The OWC reached maximum CWRs of 84%, 98% and 129% for geometry A, B and C, respectively.

Efficiencies above 100% can be expected for OWC devices excited close to their natural resonant frequency [19]. In addition, the OWC might be capturing the energy from a larger wavefront than 0.10 m (the h-WEC module is 0.40 m large), and the "tapering" effect of the side, or harbour, walls is known to significantly increase the CWR of OWC devices [19].

2) Analysis of the OTD component

The power captured by the OTD device is the sum of the power captured by each of its reservoirs, calculated as,

$$P_{OTD} = \sum_{i=1}^{n} \rho g c_i q_i \quad (2)$$

where c_i is the crest height of the ith reservoir relative to the still water level and q_i is the mean overtopping flow rate per meter of reservoir width that enters the ith reservoir. Fig. 8a shows the hydraulic efficiency of the OTD device, calculated as the ratio between the hydrodynamic power captured and wave power available, as a function of the wave period for a fixed wave height of 0.02 m. Fig. 8b shows the hydraulic efficiency of the OTD as a function of the wave height for the resonant wave period of each geometry. The wavefront considered to calculate the available wave power was 0.40 m.

Fig. 8a shows that the OTD device reached maximum hydraulic efficiencies of 36%, 29% and 25% for geometry A (T=8 s), B (T=8 s) and C (T=6 s), respectively. The three

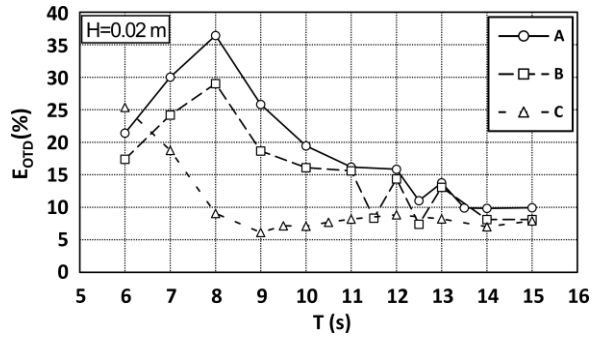

(a)

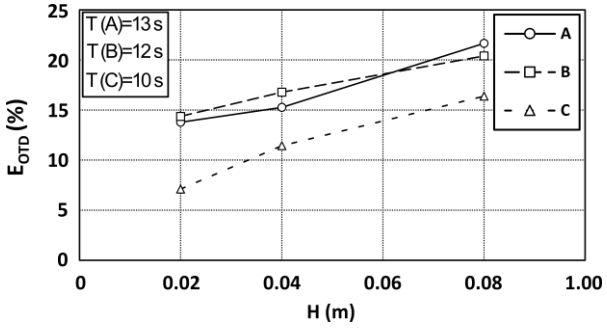

(b)

Fig. 8. Hydraulic efficiency of the OTD as a function of (a) wave period with a fixed wave height of 0.02 m and (b) as a function of the wave height for the resonant wave period of the OWC for each geometry.

geometries show higher efficiencies for the lower wave periods and somewhat lower but more constant efficiency for wave periods above 9 s.

Fig. 8b shows that the hydraulic efficiency of the OTD increases with wave height tested, although not proportionally. As can be seen in Fig. 2, the wave resource is denser for significant wave heights between 1.5 and 3.5 m. Moreover, because the crest heights of the reservoirs were optimized considering the wave resource, it is natural that the OTD component performs better for those wave heights.

3) Analysis of the h-WEC as a whole

Because the efficiencies of the OTD and OWC components are significantly different, the relative efficiency, calculated as the ratio between the efficiency and the maximum efficiency of each component and geometry, was calculated and is shown in Fig. 9. Hence, it is possible to better assess for which wave periods each component performs better. Fig. 9 shows that the OTD component (solid lines) has higher efficiencies for lower wave periods (up to around 9 s), and the OWC component (dashed lines) has greater efficiencies for higher wave periods (from 9 s for geometries B and C and 10 s for geometry A).

This shows that the h-WEC has the potential of producing electricity more constantly over a broader range of wave periods. Constant power production is a critical aspect of supplying power to electrical grids, which could be resolved, or at least enhanced, with the dual-WEC

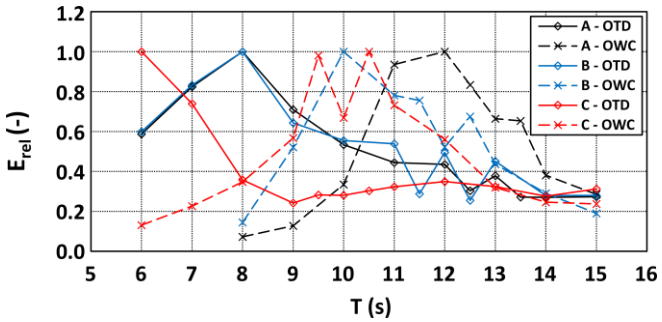

Fig. 9. Relative efficiency as a function of tested wave period.

concept. Finally, Fig. 10 shows the efficiency of the h-WEC as the sum of the efficiencies of the OTD and OWC components. Its shows that the h-WEC has a relatively constant efficiency over a broad range of wave periods.

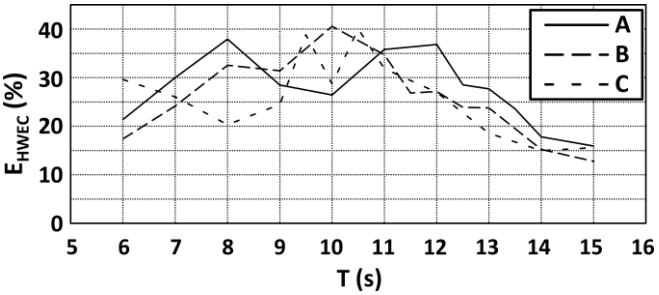

Fig. 10. Hydraulic/hydrodynamic efficiency of the h-WEC as a function of the wave period.

B. Annual Electricity Production

The Annual Electricity Production of the h-WEC device was calculated based on the tests with irregular waves, which represent 97% of the mean annual available wave resource. The efficiencies of the power conversion steps that were outside of this study were obtained from the literature. The following efficiencies were considered:

- Reservoir efficiency η_{res} (OTD - efficiency of the power conversion from the reservoir's crest to the stored water head): 75% [9, 28];
- Hydraulic turbine efficiency η_{hturb} (OTD): 80% [9, 28];
- Air turbine efficiency η_{atur} (OWC): 70% [9, 25]
- Electrical generator efficiency η_{gen} (OTD and OWC): 95% [9, 28].

The estimated energy production of the OTD and OWC components are calculated as,

$$e_{OTD} = P_{OTD} \cdot \eta_{res} \cdot \eta_{htur} \cdot \eta_{gen} \cdot h_i \cdot L_{OTD} \quad (3)$$

$$e_{OWC} = P_{OWC} \cdot \eta_{atur} \cdot \eta_{gen} \cdot h_i \cdot L_{OWC} \quad (4)$$

where P_{OWC} is the power captured by the OWC, calculated as in (1), P_{OTD} is the power captured by the OTD, calculated as in (2), h_i is the mean number of hours of occurrence of the ith condition (combination of the probabilities of

occurrence of the sea state and water level), L_{OTD} and L_{OWC} are the widths of the OTD (0.40 m) and OWC (0.10 m) components, respectively. Energy values will be presented in full-scale.

1) Selection of geometry

In order to select one of the three tested geometries of the OWC entrance and OTD frontal ramp, a preliminary test series was carried out with conditions IW1 to IW5 for the MSL, and IW1 and IW2 for the LWL and HWL. Fig. 11 shows the estimated energy captured by the h-WEC module by each geometry, as well as each component's contribution. Here, as the objective is only to compare each geometry's performance and not to calculate energy production, the energy conversion steps' efficiencies were not considered, and the results can be seen as the hydrodynamic energy captured.

Fig. 11 shows that geometry B yields the most energy captured, with 888 MWh/year, against 828 and 791 MWh/year for geometries A and C, respectively. These values only partially cover the annual available power and therefore underestimate the h-WEC energy harvesting potential but can nonetheless be used to determine that geometry B presents the best overall performance of the three tested geometries. Hence, the remaining conditions will only be tested for geometry B, to complete the Annual Electricity Production assessment.

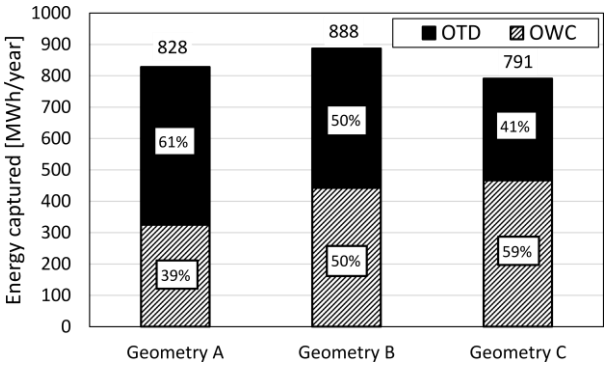

Fig. 11. Energy captured by the h-WEC for the geometry selection tests and each component's contribution.

2) Analysis of the OWC component energy production

For the sake of clarity, only the results of the best performing PTO configuration (diaphragm aperture) will be presented, in this case, 11.42 mm. Fig. 12 shows the energy produced by the OWC component of the h-WEC as a function of the condition tested, by water depth.

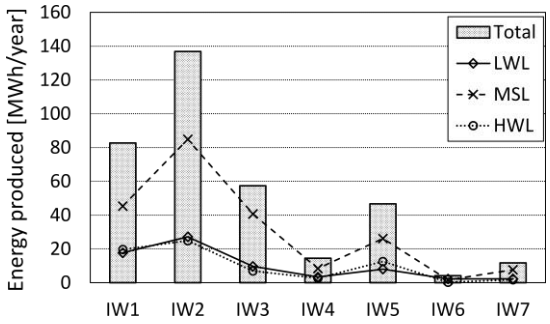

Fig. 12. Energy produced by the OWC component for each water depth tested and total.

The OWC component shows a very significant peak for condition IW2 for the three water depths and another, less prominent, peak for IW5. As IW2 represents the most significant energy contribution of the conditions tested, this peak was expected. However, IW5 represents only the fourth most significant energy contribution of the conditions tested. Moreover, the OWC shows a considerably more significant power production for conditions IW1, IW2 and IW3 compared to conditions IW4, IW5, IW6 and IW7. To better understand for which conditions the OWC performs best, the wave-to-wire efficiency of the OWC is presented in Fig. 13, calculated as the ratio between the estimated energy production and the available energy resource.

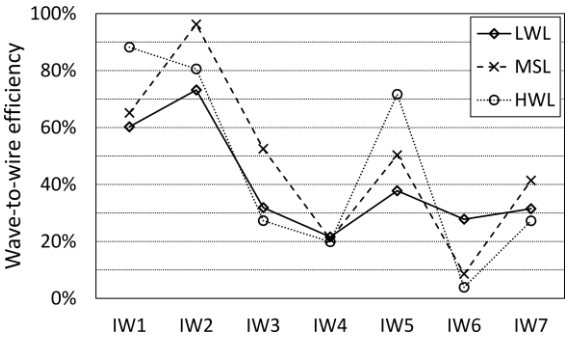

Fig. 13. Wave-to-wire efficiency of the OWC component.

The OWC's wave-to-wire efficiency shows two clear peaks, one for condition IW2 and another for IW5, the last one less pronounced. As the OWC performance is very dependent on the wave period, namely how close it is to the OWC's natural resonant period, this behaviour is due to the characteristic peak wave period of these conditions being close to the resonant wave period of the device (T_P=11.5 s and T_P=11.6 for conditions IW2 and IW5, respectively). This enhanced efficiency for IW5 also explains the energy production peak observed in Fig. 12 for the same condition. Moreover, the OWC shows good efficiencies for the other conditions with large energy contributions, namely IW1 and IW2, which shows that the device is well optimized to explore the location's resource potential. The maximum wave-to-wire efficiency was 96.2%, reached for condition IW2 and the MSL.

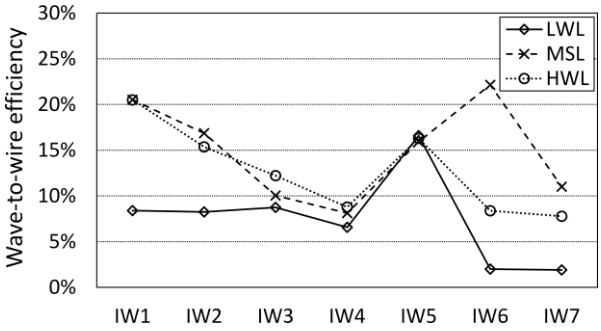

Fig. 15. Wave-to-wire efficiency of the OTD component.

3) Analysis of the OTD component energy production

Fig. 14 shows the energy produced by the OTD component of the h-WEC as a function of the condition tested, by water depth.

The OTD component shows large values of produced energy for conditions that have a more relevant energy contribution, namely IW2, similarly to the OWC. Notwithstanding, it shows almost the same energy production for condition IW1 as for condition IW2, as opposed to the OWC.

The wave-to-wire efficiency of the OTD, Fig. 15, is fairly more constant than that of the OWC. It also shows a relevant peak for IW5 and, for the MSL, a peak for IW6 (unlike the other tested depths). The maximum wave-to-wire efficiency was 22.1%, reached for condition IW6 and the MSL.

4) Analysis of the h-WEC as a whole

The estimated mean Annual Energy Production of the 20 m wide (full-scale) h-WEC is 695 MWh/year, with the OTD component yielding 341 MWh (49%) and the OWC component 354 MWh (51%), Fig. 16.

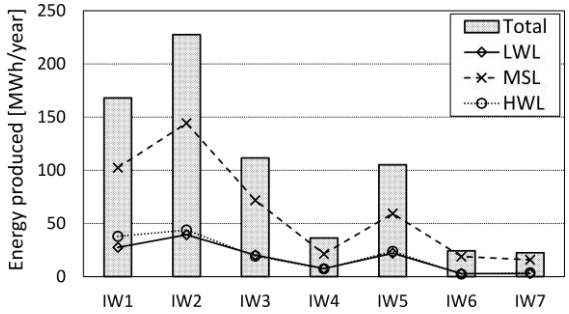

Fig. 16. Energy production of the h-WEC for each water depth and total energy production.

The estimated AEP of the h-WEC amounted to a mean power rating of almost 80 kW, which means that a 20 m wide (full-scale) device could supply more than 4% of the Port of Leixões electrical energy consumption in 2019 [29]. Moreover, if a 240 m wide device were considered, more than half of the port's electricity consumption could be supplied by the h-WEC.

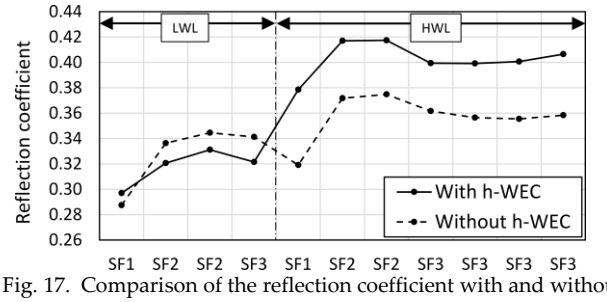

Fig. 17. Comparison of the reflection coefficient with and without the h-WEC integrated into the breakwater.

V. FUNCTIONALITY AND STABILITY OF THE NON-CONVENTIONAL BREAKWATER

The non-conventional breakwaters with integrated WECs must preserve their main function of harbour protection. This critical issue was assessed for the h-WEC integrated into the planned extension of the North breakwater of the Port of Leixões, and the results are presented hereafter.

A. Impact of the h-WEC in the breakwater's functionality

The impact of the h-WEC in the breakwater's functionality was assessed by comparing the mean overtopping flow over the structure with and without the h-WEC, as well as the reflection coefficients. The reflection coefficient, calculated as the ratio between the significant reflected wave height and the incident significant wave height, is shown in Fig. 17, with and without the h-WEC integrated. The reflection analysis was carried out using a script based on a development of the least-squares method proposed by [30].

The integration of the h-WEC into the breakwater led to slightly lower reflection coefficients for the tests with the LWL, and slightly higher reflection coefficients for the tests with the HWL. The reflection coefficients ranged from 0.29 to 0.37 without the h-WEC and 0.30 to 0.42 with the h-WEC. The introduction of the h-WEC into the breakwater does not have a significant impact on its reflection coefficient, which is natural as the h-WEC absorbs wave energy and rubble-mound breakwaters dissipate it.

Subsequentially, the mean overtopping flow rate over the structure, with and without the h-WEC, was analysed,

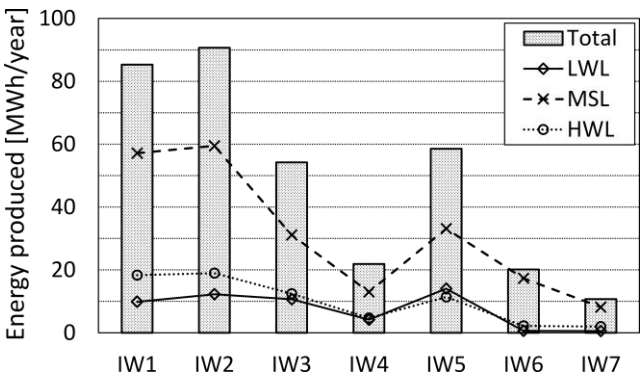

Fig. 14. Energy produced by the OTD component for each water depth tested and total.

Fig. 18. For the tests with the h-WEC, the mean overtopping flow rate was calculated only over the h-WEC module, and not the adjacent conventional breakwater on each side. All the values displayed are in full-scale.

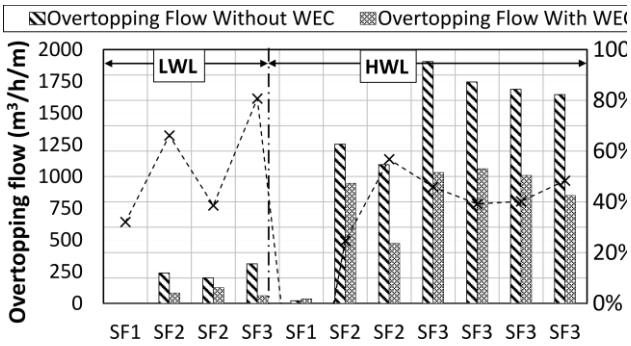

Fig. 18. Overtopping flow rate over the structure with and without the h-WEC integrated into the breakwater.

Results show that the overtopping flow decreases significantly with the h-WEC's integration, except for condition SF1 with the LWL. This outlier is attributed to the uncertainty of wave overtopping prediction for low discharge data [31] and is not considered relevant as overtopping discharges are very low both with and without the h-WEC. The average overtopping discharge reduction was 47% (excluding condition SF1-LWL), which is a notorious advantage of the breakwater-integrated h-WEC for harbour protection.

B. *Impact of the h-WEC in the stability of the breakwater's armour layer*

The stability of the breakwater was studied by tracking the movement of the armour layer blocks and the toe berm blocks after each test using a photographic camera and calculating the damage number N_{od} for each, defined as:

$$N_{od} = \frac{N_{mov}}{L/D_n} \tag{5}$$

where N_{mov} represents the number of units that moved, L the width of the reference section and D_n the nominal diameter of the Antifer blocks (the equivalent cube length in this case). No blocks of the armour layer moved; hence results are only shown for the toe berm in Fig. 19.

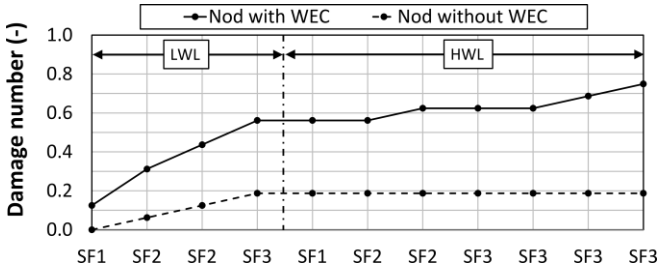

Fig. 19. Damage number N_{od} of the toe berm with and without the h-WEC integrated into the breakwater.

Results show that the damage number increased considerably with the integration of the h-WEC. After the last test, the N_{od} is almost four times larger with the h-WEC than without the h-WEC. This shows that the design of the breakwater's armour layer needs to take into consideration the effect of the h-WEC. Furthermore, as opposed to the tests without the h-WEC, the N_{od} value does not seem to have reached a stable value, given that it increased up until the last test, which could mean that damage could continue to increase, possibly leading to structural failure.

VI. Main Conclusions and Future Perspectives

A. *Main conclusions*

Physical model tests were carried out to assess the performance of a novel hybrid wave energy converter integrated into a case-study breakwater, as well as its impact on the breakwater's main function of harbour protection in terms of mean overtopping discharges, wave reflection and movement of armour layer units. The results showed that the wave energy harnessing potential of the device is good, with an estimated 695 MWh/year of electricity produced for the case-study location in the Port of Leixões, Portugal, for a 20 m wide (full-scale) device. As the planned extension of the breakwater where the device was considered to be integrated is 300 m long, if the device is used in 80% of its extension, more than half of the Port of Leixões electricity consumption in 2019 [29] could be provided by the h-WEC. Despite the encouraging results, it was determined that the integration of the h-WEC led to an increase in the damage number of the toe berm, which suggests that the design of the armour layer should be taken into consideration for breakwaters into which the h-WEC is integrated. Notwithstanding, the overtopping discharges over the structure decreased by almost 50%, and the wave reflection was not significantly affected. Ultimately, the results are favourable to the integration of the h-WEC into rubble-mound breakwaters as it showed good wave energy conversion potential and a reduced impact in the breakwater's functionality and stability.

B. *Future perspectives*

Further research is needed to increase the device's Technology Readiness Level (TRL), namely in terms of structural assessment and PTO control strategies. Wave pressures and loading in the device should be measured, and further investigations of the stability of the armour layer and the occurrence of scour in front of the structure should be conducted. These issues are being tackled in the PORTOS and WEC4PORTS projects, where a 1:40 scale re-designed device will be tested, using predictive control strategies applied to the PTO that can further increase the device's efficiency. In these projects not only the device's efficiency should be further improved, but a performance and reliability assessment of the h-WEC and its components should be performed. To reach that goal, the physical model will be equipped with pressure sensors that measure impact forces in the device, as well as pressure sensors inside the rubble-mound breakwater's internal layer to quantify the internal pressures. In

addition, a 3D laser scanner will be used to monitor the displacement of armour layer blocks between tests and the changes in the bathymetry, which will allow assessing the occurrence of scour in front of the device. The experimental data will be used to calibrate and validate numerical models.

Moreover, the device's integration into breakwaters will be optimized to minimize costs and reduce the LCoE, thus leveraging the overall economics of upfront CAPEX. To achieve this ambitious goal, state-of-the-art CFD codes will be used to improve the h-WEC's overall efficiency alongside the reduced-scale physical modelling performed at the University of Porto to analyse the device's impact on the breakwater's functionality and stability, as well as the survivability of the whole solution. Finally, a new OWC turbine will be designed and tested at the Mutriku test site. What is more, a new material will be tested on-site to assess its strength and ability to withstand harsh marine conditions. The full-scale testing of key components of the device is a critical factor to increase the technology's TRL and allows to assess and improve installation, operation, and maintenance procedures of these complex power conversion systems, as well as obtaining a realistic estimation of their performances.

Acknowledgement

The authors are in debt to LNEC (*Laboratório Nacional de Engenharia Civil*), which lent the Antifer units used to materialize the armour layer of the reference breakwater model, to INEGI, who produced the h-WEC model, and to APDL, for all the information provided to characterize the case study breakwater. Prof. João Henriques (from *Instituto Superior Técnico*) provided important contributions to the testing and control of the PTO system used in the OWC module. The authors would also like to thank the support of the staff of the Hydraulics Laboratory of FEUP, Mr. Miguel Guerra, during the experiments.

References

[1] European Commission, "The European green deal," in *Communication form the Commission to the European Parliament, the European Council, the Council, the European Economic and Social Committee and the Committee of the Regions*, ed, 2019.

[2] J. Cruz, "Ocean Wave Energy: Current Status and Future Perspectives," pp. 287-385, 01/01 2008.

[3] B. Drew, A. R. Plummer, and M. N. Sahinkaya, "A review of wave energy converter technology," *Proceedings of the Institution of Mechanical Engineers, Part A: Journal of Power and Energy,* vol. 223, no. 8, pp. 887-902, 2009, doi: 10.1243/09576509jpe782.

[4] X. L. Zhao, D. Z. Ning, Q. P. Zou, D. S. Qiao, and S. Q. Cai, "Hybrid floating breakwater-WEC system: A review," *Ocean Engineering,* vol. 186, p. 106126, 2019/08/15/ 2019, doi: https://doi.org/10.1016/j.oceaneng.2019.106126.

[5] L. Victor, P. Troch, and J. P. Kofoed, "On the Effects of Geometry Control on the Performance of Overtopping Wave Energy Converters," *Energies,* vol. 4, no. 10, 2011, doi: 10.3390/en4101574.

[6] D. Vicinanza, L. Margheritini, J. P. Kofoed, and M. Buccino, "The SSG Wave Energy Converter: Performance, Status and Recent Developments," *Energies,* vol. 5, no. 2, p. 193, 2012. [Online]. Available: http://www.mdpi.com/1996-1073/5/2/193.

[7] P. Oliveira, F. Taveira-Pinto, T. Morais, and P. Rosa-Santos, "Experimental evaluation of the effect of wave focusing walls on the performance of the Sea-wave Slot-cone Generator," *Energy Conversion and Management,* vol. 110, pp. 165-175, 2016/02/15/ 2016, doi: https://doi.org/10.1016/j.enconman.2015.11.071.

[8] T. Calheiros-Cabral, D. Clemente, P. Rosa-Santos, F. Taveira-Pinto, F. Belga, and T. Morais, "Preliminary assessment of the impact of a Hybrid Wave Energy Converter in the stability and functionality of a rubble-mound breakwater," in *Coastal Structures 2019*, Hannover, Germany, 2019, doi: 10.18451/978-3-939230-64-9_114.

[9] T. Calheiros-Cabral *et al.*, "Performance Assessment of a Hybrid Wave Energy Converter Integrated into a Harbor Breakwater," *Energies,* vol. 13, no. 1, p. 236, 2020, doi: https://doi.org/10.3390/en13010236.

[10] T. Calheiros-Cabral *et al.*, "Evaluation of the annual electricity production of a hybrid breakwater-integrated wave energy converter," *Energy,* vol. 213, p. 118845, 2020/12/15/ 2020, doi: https://doi.org/10.1016/j.energy.2020.118845.

[11] P. Rosa-Santos *et al.*, "Experimental Study of a Hybrid Wave Energy Converter Integrated in a Harbor Breakwater," *Journal of Marine Science and Engineering,* vol. 7, no. 2, p. 33, 2019, doi: 10.3390/jmse7020033.

[12] N. Booij *et al.*, "SWAN Technical Documentation, Cycle III, version 40.51," ed. Delft, The Netherlands: Delft University of Technology, 2006.

[13] R. Capitão, L. Pinheiro, and C. J. Fortes, "Estudos em modelo físico e numérico do prolongamento do quebra-mar exterior e das acessibilidades marítimas do porto de Leixões. Estudo I - Regimes de agitação marítima," LNEC, Lisboa, Portugal, 2017.

[14] A. Pecher and J. P. Kofoed, *Handbook of Ocean Wave Energy*. Cham: Springer International Publishing, 2017, pp. E1-E1.

[15] European Commission, "Working group ocean energy, SET-plan ocean energy implementation plan," 2018.

[16] J. P. Kofoed, "Wave Overtopping of Marine Structures: utilization of wave energy," PhD, Department of Civil Engineering, Aalborg University, Series Papers, No. 24, 2002.

[17] T. Calheiros-Cabral, "Avaliação do desempenho de um sistema híbrido de aproveitamento da energia das ondas para o quebramar Norte de Leixões," MSc, Civil Engineering Department, Faculdade de Engenharia da Universidade do Porto, Porto, Portugal, 202119939, 2018. [Online]. Available: https://hdl.handle.net/10216/114537

[18] P. Meinert, L. Gilling, and J. P. Kofoed, "User manual for SSG Power simulation 2 ", ed. Hydraulics and Coastal Engineering No. 44, Aalborg, Denmark, 2008.

[19] D. Raj, V. Sundar, and S. A. Sannasiraj, "Enhancement of hydrodynamic performance of an Oscillating Water Column with harbour walls," *Renewable Energy,* vol. 132, pp. 142-156, 2019/03/01/ 2019, doi: https://doi.org/10.1016/j.renene.2018.07.089.

[20] ANSYS, "ANSYS Fluent Theory Guide; Release 15.0," ed. Canonsburg, PA, USA: ANSYS, 2013, p. 780.

[21] P. Contestabile, F. Vincenzo, E. Di Lauro, and D. Vicinanza, "Full-scale prototype of an overtopping breakwater for wave energy conversion," *2017,* OBREC; innovative breakwater; overtopping wave energy converter; full-scale device no. 35, 2017-06-23 2017, doi: 10.9753/icce.v35.structures.12.

[22] I. Crema, I. Simonetti, L. Cappietti, and H. Oumeraci, "Laboratory Experiments on Oscillating Water Column Wave Energy Converters Integrated in a Very Large Floating Structure," in *European Wave and Tidal Energy Conference*, Nantes, France, 6-11 September 2015 2015.

[23] V. Heller, "Scale effects in physical hydraulic engineering models," *Journal of Hydraulic Research,* vol. 49, no. 3, pp. 293-306, 2011/06/01 2011, doi: 10.1080/00221686.2011.578914.

[24] A. F. O. Falcão and J. C. C. Henriques, "Model-prototype similarity of oscillating-water-column wave energy converters," *International Journal of Marine Energy,* vol. 6, pp. 18-34, June 2014 2014, doi: 10.1016/j.ijome.2014.05.002.

[25] A. F. O. Falcão, L. M. C. Gato, and E. P. A. S. Nunes, "A novel radial self-rectifying air turbine for use in wave energy converters. Part 2. Results from model testing," *Renewable Energy,* vol. 53, pp. 159-164, 2013/05/01/ 2013, doi: https://doi.org/10.1016/j.renene.2012.11.018.

[26] A. Elhanafi and C. J. Kim, "Experimental and numerical investigation on wave height and power take–off damping effects on the hydrodynamic performance of an offshore–stationary OWC wave energy converter," *Renewable Energy,* vol. 125, pp. 518-528, 2018/09/01/ 2018, doi: https://doi.org/10.1016/j.renene.2018.02.131.

[27] C. Perez-Collazo, D. Greaves, and G. Iglesias, "Hydrodynamic response of the WEC sub-system of a novel hybrid wind-wave energy converter," *Energy Conversion and Management,* vol. 171, pp. 307-325, 2018/09/01/ 2018, doi: https://doi.org/10.1016/j.enconman.2018.05.090.

[28] L. Margheritini, "R&D Towards Commercialization of Sea Wave Slot Cone Generator (SSG) Overtopping Wave Energy Converter: selected topics in the field of wave energy," 2009.

[29] APDL, "Relatório de sustentabilidade 2019," 2019. Accessed: 15 April 2021.

[30] E. P. D. Mansard and E. R. Funke, "The Measurement of Incident and Reflected Spectra Using a Least Squares Method," in *Coastal Engineering 1980*, 1980, pp. 154-172.

[31] A. Romano, G. Bellotti, R. Briganti, and L. Franco, "Uncertainties in the physical modelling of the wave overtopping over a rubble mound breakwater: The role of the seeding number and of the test duration.," *Coast. Eng.,* vol. 103, pp. 15-21, 2015.